Estimation of carbon content and dissolved organic matter in inland waters using EnMAP hyperspectral imaging

Bárbara Alvado[1], Xavier Sòria-Perpinyà[1], Antonio Ruíz-Verdú[1], Gabriel Caballero[1], Jesús Delegido[1], Juan Miguel Soria[2], Eduardo Vicente[2], José Moreno[1], María Antonia Rodrigo[2]

1 Image Processing Laboratory, Parc Científic Universitat de València, Edifici E4, 4ª planta, C/Catedrátic Agustín Escardino, 9, 46980 Paterna (España), Barbara.Alvado@uv.es, Javier.Soria-Perpina@uv.es, Antonio.Ruiz@uv.es, Gabriel.Caballero@uv.es, Jesus.Delegido@uv.es, Jose.Moreno@uv.es
2 Cavanilles Institute of Biodiversity and Evolutionary Biology (ICBiBE), Parc Científic Universitat de València, C/Catedrátic José Beltrán Martínez, 2, 46980 Paterna (España), Juan.Soria@uv.es, Eduardo.Vicente@uv.es, Maria.A.Rodrigo@uv.es

Keywords: total organic carbon, dissolved organic carbon, particulate organic carbon, colored dissolved organic matter, EnMAP.

Abstract

Inland water bodies, despite occupying a small fraction of the Earth's Surface, play a significant role as carbon sinks or emitters of carbon dioxide and other greenhouse gases. Remote sensing has the potential to provide continuous carbon estimates; however, conventional operational missions are currently limited by the number of bands, which hinders the detailed detection of certain peaks in reflectance spectra. The hyperspectral EnMAP sensor provides images with 260 bands and a spatial resolution of 30 m. The objective of this study is to estimate the carbon content in continental water bodies of the eastern Iberian Peninsula (Spain), with varying trophic states, through four variables: total organic carbon (TOC), dissolved organic carbon (DOC), particulate organic carbon (POC), and colored dissolved organic matter (CDOM). Different indices and combinations of bands have been studied, based on in situ measurements of these variables coinciding with the acquisition of EnMAP images. The results show that TOC, can be estimated with a triband index using the 525, 535 and 551 nm bands (R^2 = 0.96) and an exponential fitting curve; DOC with a normalized difference using the 599 and 525 nm bands (R^2 = 0.93) with an exponential fitting curve; CDOM with simple ratio between bands 435 and 721 (R^2 = 0.95) with a linear fitting curve. POC is calculated as the difference between TOC and DOC (R^2 = 0.86).

1. Introduction:

The role of inland waters in the global carbon (C) cycle was considered insignificant until just over a decade ago. However, these systems can act as C sinks, as phytoplankton, algae, and aquatic plants assimilate atmospheric carbon dioxide (CO_2) during primary production. Under climate change scenarios characterized by rising temperatures and increasing eutrophication, these water bodies may shift from carbon sinks to carbon sources due to imbalances between respiration and primary production. Furthermore, they may become significant emitters of greenhouse gases such as methane (CH_4) (Williamson et al., 2008, Vanderklift et al., 2019). Therefore, the quantification and characterization of carbon in its various fractions is essential to elucidate the role of inland waters in the global carbon cycle.

C is present in aquatic systems as dissolved CO_2, bicarbonate (HCO_3^-), and carbonate (CO_3^{2-}), in varying proportions. The particulate (POC) and dissolved (DOC) organic carbon represent the two components of the total organic carbon (TOC) pool in water (Bonelli et al., 2022). This organic matter can either undergo decomposition or persist, accumulating in sediments. DOC can affect aquatic ecosystems through its capacity to interact with heavy metals and hydrophobic pollutants, altering their bioavailability (Spencer et al., 2012). This can enhance the transport of contaminants to other areas or lead to their accumulation in enclosed ecosystems. In contrast, the decomposition of POC consumes oxygen; at high concentrations, it can lead to hypoxic or anoxic conditions (Zhou et al., 2023). The light-absorbing fraction of DOC is the colored dissolved organic matter (CDOM), which strongly absorbs light in the ultraviolet and blue region (Tehrani et al., 2013). At high concentrations, CDOM warms the surface layer of water, accentuating stratification and hindering the vertical mixing of nutrients and oxygen. Furthermore, by reducing light penetration, it can limit photosynthesis in surface layers, favoring species adapted to low light conditions.

Remote sensing has the potential to provide continuous high-resolution optical observations that could be used to estimate the carbon pools in water. Nevertheless, recent studies have focused more on oceanic and coastal environments than on inland water, particularly those of small size. In addition, these studies have developed algorithms to estimate carbon content using multispectral sensors (Odermatt et al., 2012, Tehrani et al., 2013, Kutser et al., 2015, Cherukuru et al., 2016). However, hyperspectral satellite data offer more detailed information on the physical properties of water, such as reflectance, absorption, and emission (Krutz et al., 2019), which can be used to develop more accurate algorithms for assessing water quality (Hestir et al., 2015).

The Environmental Mapping and Analysis Program (EnMAP) scientific mission, in orbit since 2022, is a hyperspectral sensor with 260 bands covering the 420-2450 nm range, with a spatial resolution of 30 m. It has a global revisit capability of 21 days, although for specific targets, this period can be reduced to 3-4 days, which may be of interest for scientific studies. Table 1 summarizes the main characteristics of the EnMAP sensor.

Parameter		Value
Spectral range	VNIR	420 – 1000 nm
	SWIR	900 – 2450 nm
Spectral channels		228
Spectral resolution	VNIR	5 nm
	SWIR	10 nm
Signal to Noise Ratio		>500:1 400 – 1000 nm
Spatial resolution		30 m
Swath Width		30 km
GSD		30 m

Table 1. EnMAP parameters (modified from Kaufmann et al., 2016).

Given the growing interest in hyperspectral missions, especially the future missions being planned by the Copernicus program of the European Space Agency, new perspectives in water quality studies are being opened. Therefore, the objective of this work is to develop algorithms for estimating TOC, DOC, POC and CDOM using EnMAP images, in order to assess the carbon content in continental water bodies.

2. Methodology:

2.1 Study area

In this study, field campaigns were conducted across several inland water masses in the Valencian Community (Spain), with a diverse range of physical characteristics and trophic states (figure 1). Three of the sites (Benagéber, Tous and Sitjar) are oligotrophic, characterized by clear, transparent waters. In contrast, the remaining sites (Bellús, Beniarrés and Albufera) are eutrophic. Eutrophic conditions in these waters are primarily attributed to their proximity to densely populated areas with significant industrial and/or agricultural activity. These anthropogenic inputs result in elevated nutrient loads, promoting excessive phytoplankton growth and consequently leading to high turbidity levels.

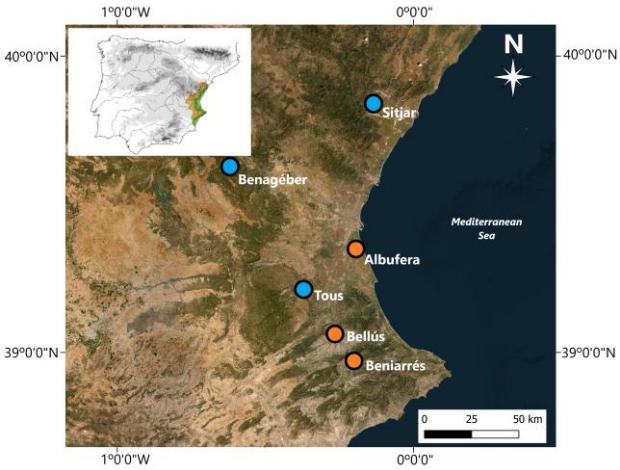

Figure 1. Location of selected water masses in the eastern region of the Iberian Peninsula (Spain). The orange dots correspond to waters with eutrophic status, and the blue dots correspond to those with oligotrophic status.

2.2 Field campaigns and laboratory analysis

For calibration and validation of remote sensing algorithms, the most widely used approach involves the simultaneous measurement of in situ data during satellite overpasses. Between 2023 and 2024, eight field campaigns were conducted, obtaining 23 georeferenced water samples. The campaigns were planned to coincide with satellite imagery acquisition on cloud-free days within a suitable temporal window. Nevertheless, in some cases, the time interval between satellite overpass and sample collection was extended to ±3 days (Schröder et al., 2024), due to the use of archived imagery.

On each campaign, samples were collected over different locations of the water masses (2 to 5 points), at a minimum distance of 100 m from the shoreline to avoid mixed pixels or adjacency effects. Using a Secchi disk, water transparency was measured and, taking as a reference the depth at which the disk was no longer visible (Secchi disk depth, SDD), water samples were taken. In turbid waters with lower SDD, a Ruttner bottle was used, while in clear waters with a higher SDD, a weighted PVC tube was used. The collected samples were then refrigerated and kept in darkness for transport to the laboratory.

To determine the different carbon components, we begin by filtering an adequate volume of water through a Whatman GF/F type glass fiber filter that retains the total suspended solids. Next, we separately analyze the filtered water for DOC. We do this using a SHIMADZU TOC-V CSN carbon analyzer with an ASI-V autosampler, which directly measures its concentration in the water.

To measure the TOC, we use unfiltered water, separating an appropriate amount into glass tubes and treating it with ultrasound for 15 minutes in a BRANSON 2800 sonicator, to homogenize any particulate matter it contains. Once the sample is homogenized and placed in the analysis vials, we add a mini magnetic stirrer, which ensures sample homogeneity throughout the analysis process. We do this using the aforementioned SHIMADZU TOC-V CSN carbon analyzer. Once the analysis is complete, we collect the data at the TOC column.

CDOM was determined by UV spectrophotometry using a 10 nm optical path quartz cuvette. Then, it was calculated at 250 nm using a quinine sulfate standard curve, as described in Hoge et al. (1993).

2.3 Image processing

For this study, eight EnMAP L2A images were used. These images include sensor-specific atmospheric correction with good validation results, as stated in Alvado et al. (2024). Table 2 summarizes the information from the image acquisition and field campaigns.

Reservoir	Samples	Date	Time window
Albufera	1	2023/04/20	3
Benagéber	1	2024/04/22	Match
Albufera	5	2024/07/19	Match
Tous	3	2024/07/19	Match
Bellús	3	2024/07/23	Match
Beniarrés	2	2024/07/23	Match
Albufera	5	2024/07/31	Match
Sitjar	3	2024/07/31	Match

Table 2. EnMAP acquisition and field campaigns. "Match" means that the field campaign was conducted on the same day as the satellite overpass.

Atmospherically corrected images were processed using SNAP (Sentinel Application Platform) software. As part of this process, the spectra of a 3x3 pixel window, centered on each sampling point, were extracted to calculate the average reflectance values for each spectral band. As the values provided by EnMAP images are reflectance values (R), they were converted to Remote sensing reflectance (Rrs) by dividing by π.

2.4 Algorithm retrieval

Using the free software ARTMO (Automated Radiative Transfer Models Operator), all possible band combinations can be defined and evaluated in different ways, allowing mathematical combinations of Rrs

measured in different wavelength ranges, to be correlated with biophysical variables of interest. Simple ratio (SR: Rrs1/Rrs2), normalized difference (ND: (Rrs2 – Rrs1)/(Rrs2 + Rrs1)) and triband (Rrs1 x ((1/Rrs2) – (1/Rrs3))) formulations have been used. Several fitting functions (linear, exponential, potential and logarithmic) have been tested to obtain the best correlations. Using the cross-validation tool "leave-one-out", the data is divided into n parts, with one part used for model validation and the rest for calibration. The process is repeated with each of the parts, and the statistical averages are calculated.

Since ARTMO calculates various possibilities, the models with the highest coefficient of determination (R^2) were selected. Finally, to evaluate the performance of the selected models, comparisons were made with the values obtained in situ using the statistics described in Table 3.

Statistical metric	Equation
	$\varepsilon_i = x_i - y_i$
Bias	$\frac{1}{N}\sum_{i=1}^{N}\varepsilon_i$
RMSE	$\sqrt{\frac{1}{N}\sum_{i=1}^{N}(\varepsilon_i)^2}$
NRMSE	$(\frac{RMSE}{x_{i\,max} - x_{i\,min}})x100$

Table 3. Statistical metrics used to validate algorithms. x_i and y_i are the in situ data and the estimated data, respectively.

Once the best algorithm was selected, to visualize the applicability of the model, we created thematic maps that allow us to observe the spatial distribution of the variables.

3. Results & discussion

Hyperspectral satellites, with a narrower bandwidth, allow the detection of narrow peaks and troughs in the Rrs spectra. Figure 2 shows the spectra of three water masses in the study, whose optical characteristics represent the trophic states mentioned above. These water masses present a different trophic state, but all have in common phytoplankton as the dominant OAC (optically active component), contributing to the Rrs.

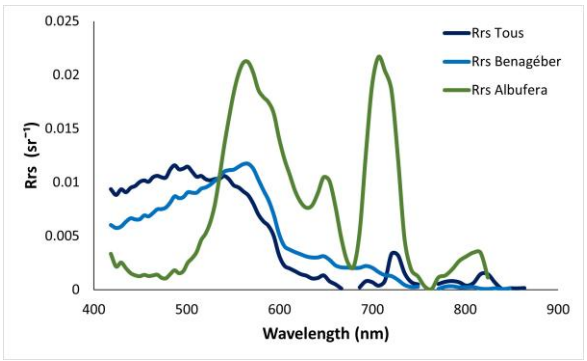

Figure 2. EnMAP spectra of water masses with different trophic status. Each spectrum corresponds to the average of the points measured in each reservoir.

Tous reservoir is ultraoligotrophic, with very clear waters and a maximum Rrs around 490 nm. From 550 nm onwards, the Rrs begins to decrease until it reaches 0 in the NIR region. However, some peaks are observed at 730 and 820, possibly due to an error in atmospheric correction.
The Benagéber reservoir, on the other hand, is oligotrophic with clear waters and a maximum of Rrs around 550 nm, as it is dominated by phytoplankton. Finally, the Albufera lagoon is hypereutrophic. In this spectrum, the maxima are around 580 nm and 715 nm (particle scattering, mainly phytoplankton), and the minima around 620 nm (Phycocyanin) and 680 (Chlorophyll-a).

TOC values measured in the laboratory ranged from 1 to 25.5 mg/L. The model that exhibited the strongest correlation with the in situ data was the triband model, based on reflectance at 525, 535, and 551 nm (figure 3, eq. 1):

$$TOC\ (mg/L) = 1.94e^{9.37\,x\,(R525\,x\,(\frac{1}{R535} - \frac{1}{R551}))} \quad (1)$$

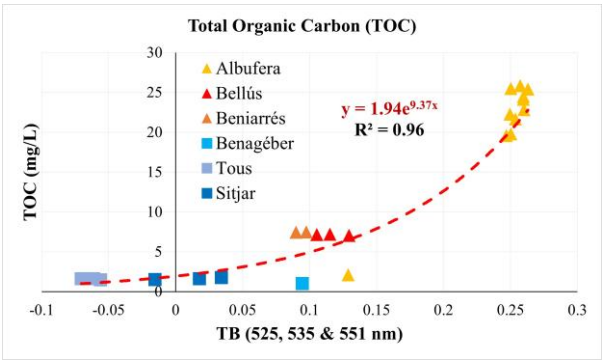

Figure 3. Adjustments between the TB index obtained with EnMAP Rrs (x-axis) and TOC measured in situ (y-axis).

The model developed for estimating TOC has an acceptable error of 9% and underestimates the values obtained according to the bias results (figure 4). Since TOC is usually composed largely of substances that absorb light in the blue regions, the green region becomes more dominant in the spectral signature. In their study, Quevedo-Castro et al. (2024) used Landsat-8 data to estimate TOC in the Sanalona reservoir (Mexico), where values range from 3.5 to 7 mg/L. Using the blue (B2) and green (B3) bands, they developed a model with an $R^2 = 0.57$.

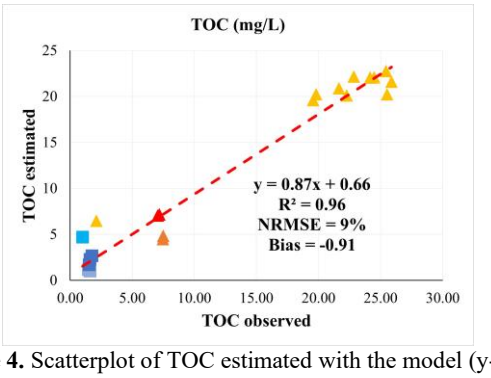

Figure 4. Scatterplot of TOC estimated with the model (y-axis) and TOC measured in situ (x-axis).

For DOC, the values analyzed in the laboratory are between 0.8 and 18.5 mg/L. Normalized difference using reflectance of 599 and 525 nm showed the best correlation with the in situ data (figure 5).

This contribution has been peer-reviewed. The double-blind peer-review was conducted on the basis of the full paper.
https://doi.org/10.5194/isprs-annals-X-3-W3-2025-3-2026 | © Author(s) 2026. CC BY 4.0 License.

$$DOC\ (mg/L) = 3.32e^{3.54\,x\,\left(\frac{R599 - R525}{R599 + R525}\right)} \quad (2)$$

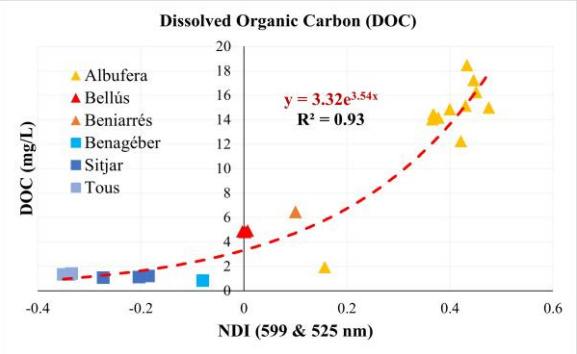

Figure 5. Adjustments between the NDI index obtained with EnMAP Rrs (x-axis) and DOC measured in situ (y-axis).

The model (figure 6) has a relative error of 10% and underestimates the measured values. It uses bands in the green and red region, as these bands are less affected by absorption. In a study conducted in Estonian lakes, where DOC concentrations range from 6.04 to 20.9 mg/L, Toming et al. (2016) developed a model using Sentinel-2 (S2) bands (L2A level). The bands selected for this model were B3 (green) and B4 (red), obtaining an R^2 = 0.42. Meanwhile, Shao et al. (2016), using field radiometry (ASD Field Spec FR spectroradiometer), obtained a model using reflectance at 643 nm and 591 nm with an R^2= 0.87.

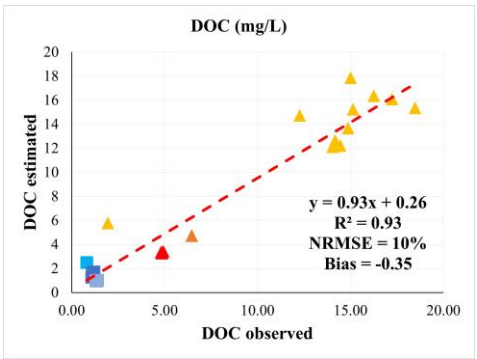

Figure 6. Scatterplot of DOC estimated with the model (y-axis) and DOC measured in situ (x-axis).

CDOM values measured in the laboratory are between 0.7 and 7.9 mg/L. The model that shows the best correlation with the in situ data is the simple ratio using reflectance at 435 and 721 nm (figure 7, eq 3):

$$CDOM\ (mg/L) = -2.08\ x\ \frac{R435}{R721} + 6.93 \quad (3)$$

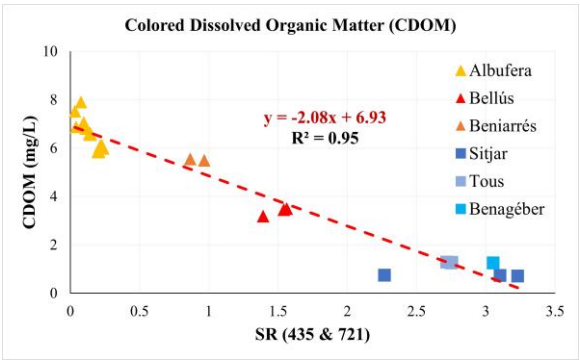

Figure 7. Adjustments between the SR index obtained with EnMAP Rrs (x-axis) and CDOM measured in situ (y-axis).

The model uses a blue band, where there is greater absorption by CDOM, and a red-edge band where CDOM absorption is negligible. The negative correlation shown in Figure 7 indicates that the higher the red-edge reflectance, the higher the CDOM concentration. This is due to the high correlation of CDOM and phytoplankton biomass in the dataset, with the phytoplankton dominating the Rrs signal. In similar water types (phytoplankton-dominated), the CDOM model could be applicable, but in CDOM-dominated waters (with low Chl-a), it could underestimate the actual CDOM concentration.

The model (figure 8) obtains estimation errors of 8% and the bias indicates that it slightly underestimates the results. Wong et al. (2020), using S2 data obtained good correlation (R^2 = 0.86) with B2 (blue) and B4 (red) in coastal waters of Singapore. Zhang et al. (2021) used the same bands in a study of a reservoir in China. In their case, the model used obtained a correlation of R^2 = 0.71.

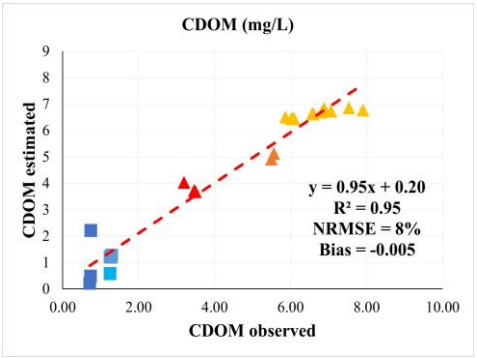

Figure 8. Scatterplot of CDOM estimated with the model (y-axis) and CDOM measured in situ (x-axis).

The POC in situ has been calculated as the difference between TOC in situ and DOC in situ with values ranging from 0.2 to 11 mg/L. The estimation of POC has been calculated as the difference between equation 1 and 2, and validation has been done fitting the data using the least squares method with a linear function (figure 9).

$$POC\ (mg/L) = 0.8287\ x\ (TOC\text{-}DOC) + 0.1152 \quad (4)$$

This contribution has been peer-reviewed. The double-blind peer-review was conducted on the basis of the full paper.
https://doi.org/10.5194/isprs-annals-X-3-W3-2025-3-2026 | © Author(s) 2026. CC BY 4.0 License.

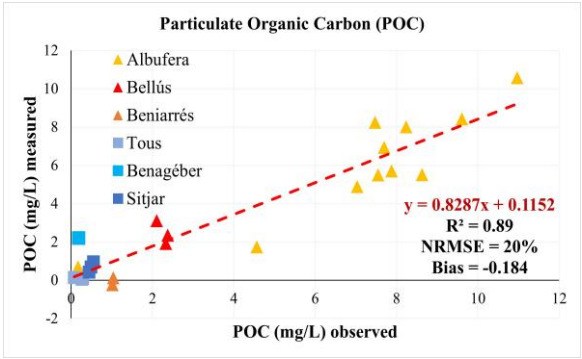

Figure 9. POC measured as the difference between TOC and DOC.

As an example, Figures 10-17 show the thematic maps obtained for each variable by applying Equations 1-4 to EnMAP images. The results obtained show how the application of the equations results in coherent thematic maps.
The selected date (2024/07/31) corresponds to a field campaign where two reservoirs with different trophic status were sampled, allowing us to see the difference in magnitude of the variables studied. Higher values were found in Albufera and lower values in Sitjar. To adapt to the study area, a water mask was created, allowing us to apply the algorithms only to water masses.

In the lagoon, the TOC and DOC variables appear homogeneous. The POC concentrations are highest along the shore, where the ditches are located, where water inflows likely contain particles. While the DOC presents higher values in the central part of the lagoon, related to greater presence of phytoplankton.

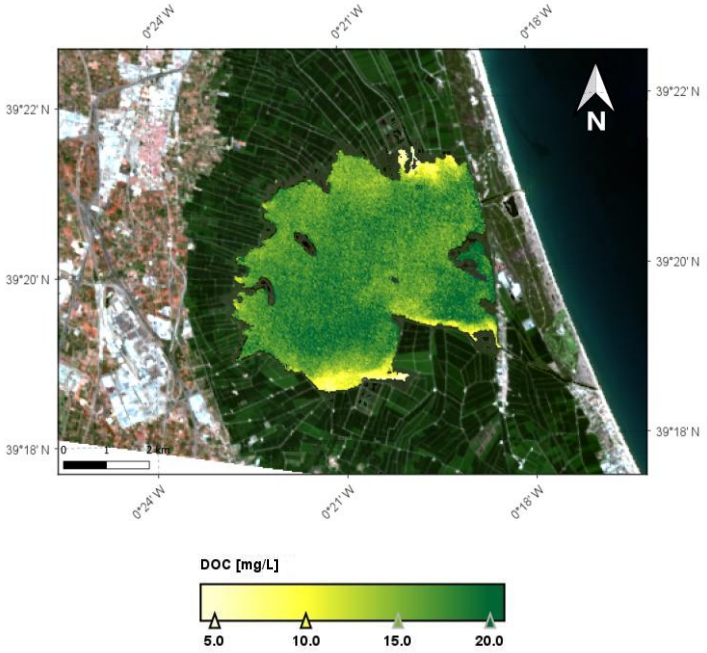

Figure 11. Estimation map of DOC (mg/L) in Albufera lagoon.

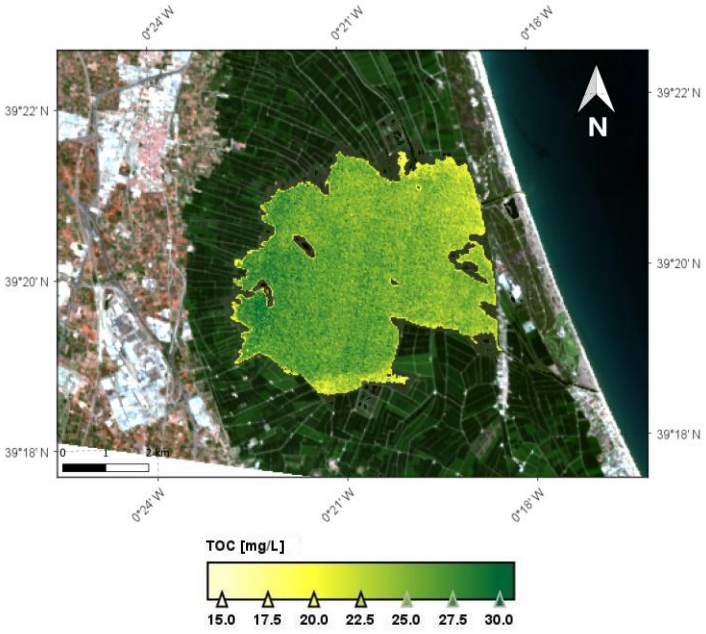

Figure 10. Estimation map of TOC (mg/L) in Albufera lagoon.

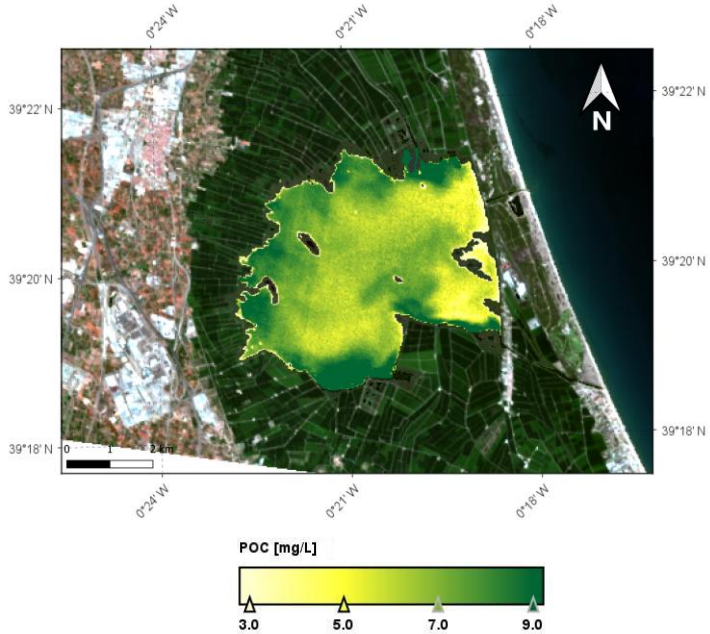

Figure 12. Estimation map of POC (mg/L) in Albufera lagoon from eq. 1 – eq. 2.

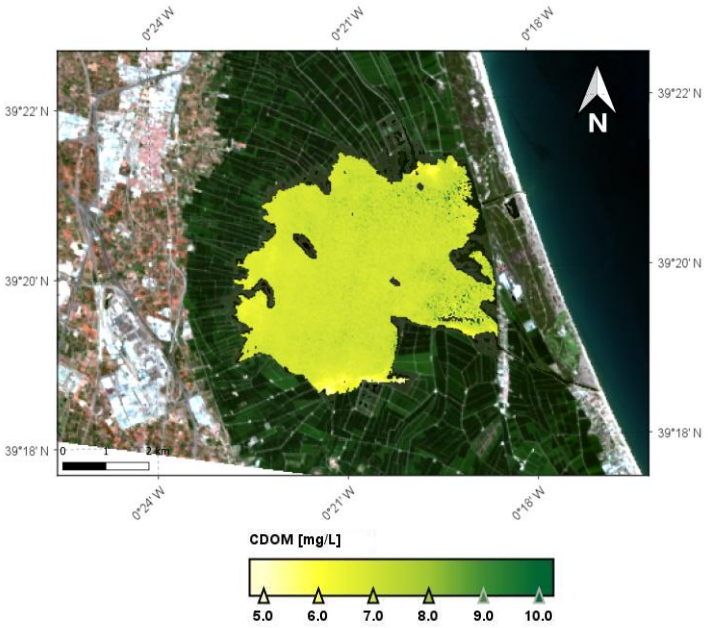

Figure 13. Estimation map of CDOM (mg/L) in Albufera lagoon.

In the case of the Sitjar reservoir, except for the POC, which appears to present more homogeneous values, the remaining variables reflect a tailwater-dam asymmetry. Thus, there is a decrease in values toward the dam, demonstrating the purification effect of the reservoirs.

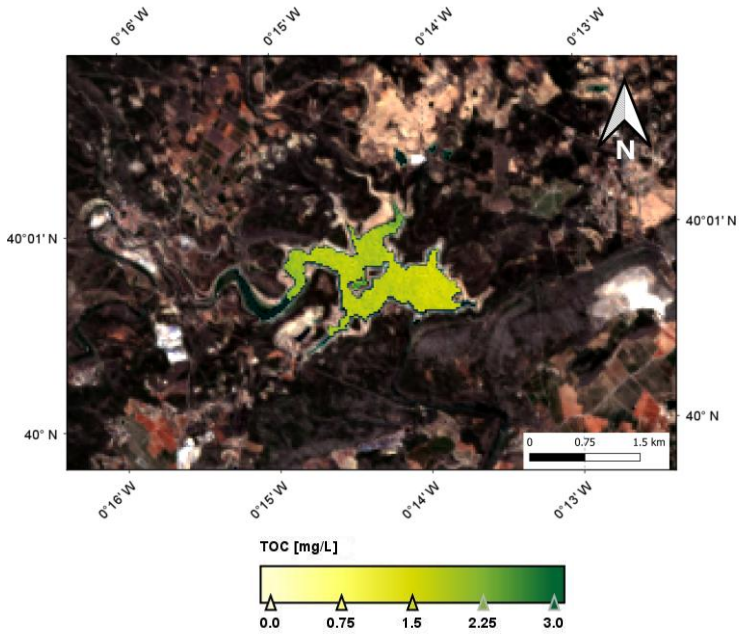

Figure 14. Estimation map of TOC (mg/L) in Sitjar reservoir.

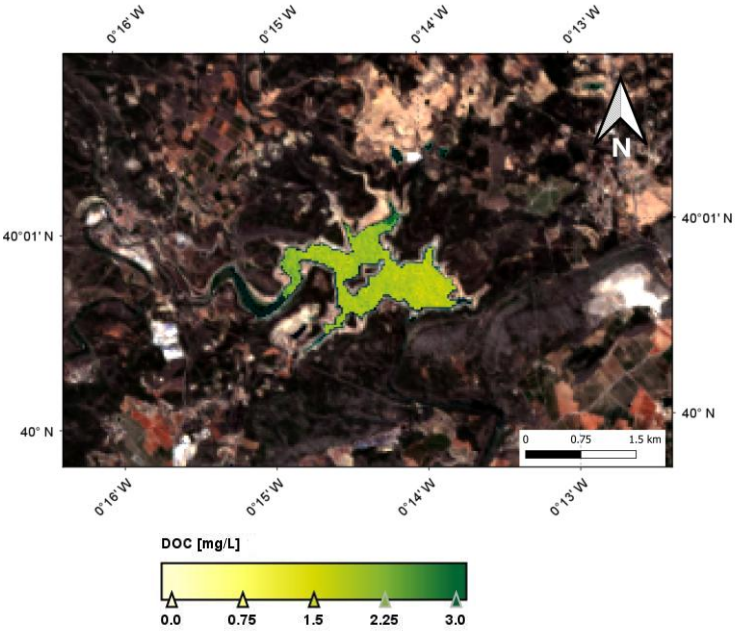

Figure 15. Estimation map of DOC (mg/L) in Sitjar reservoir.

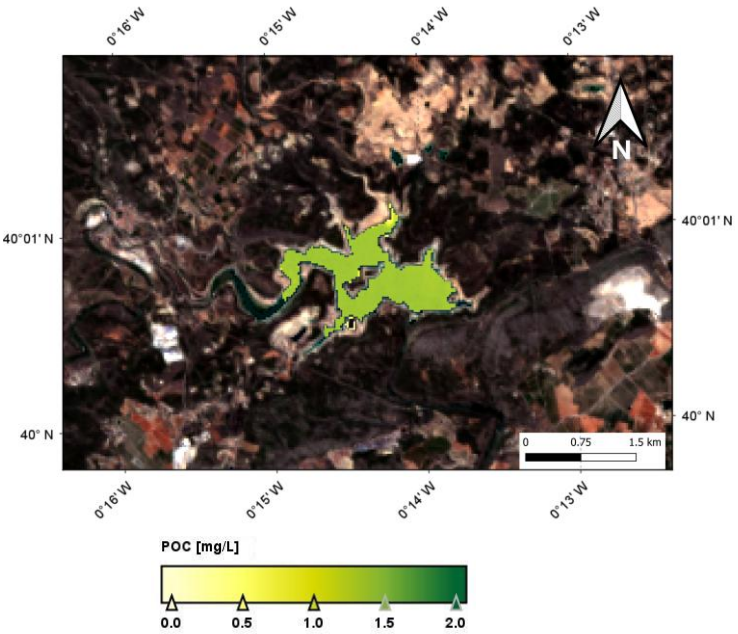

Figure 16. Estimation map of POC (mg/L) in Sitjar reservoir from eq. 1 – eq. 2.

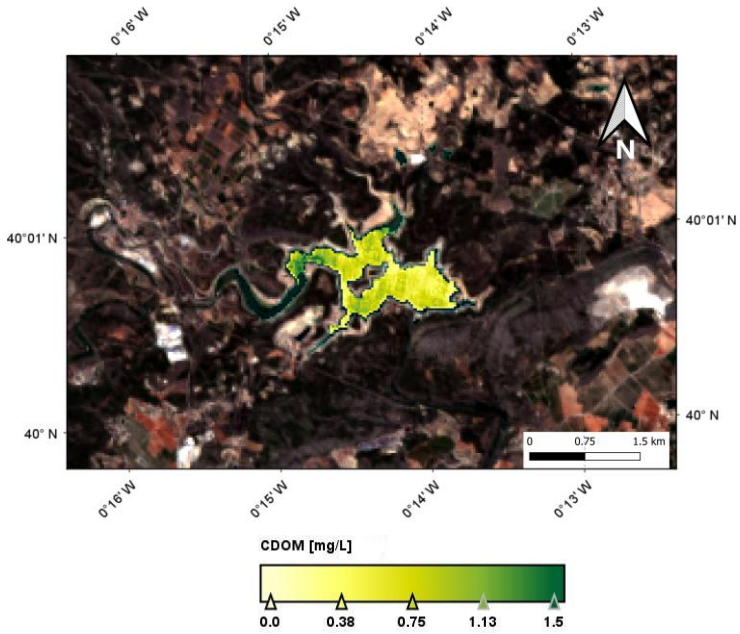

Figure 17. Estimation map of CDOM (mg/L) in Sitjar reservoir.

4. Conclusions

Our results have shown the potential of hyperspectral remote sensing to estimate carbon pools, differentiating the TOC and its components (DOC, POC, and CDOM), being able to map them to provide their spatial and temporal variations.

TOC can be estimated with an exponential relationship, using a triband model based on reflectance at 525, 535, and 551 nm, with R^2 of 96. DOC can be estimated with an exponential relationship using a normalized difference based on reflectance 599 and 525, with R^2 of 93. Based on the difference between the TOC and DOC estimation, POC can be estimated with R^2 of 89. Finally, CDOM can be estimated with a linear relationship with the ratio between 435 and 721 bands, with R^2 of 95. These band combinations allow us to capture the optical variations associated with different types of organic carbon, showing that the blue and green bands are particularly sensitive to the absorption properties of CDOM and TOC, while the red and red-edge bands are less affected by absorption.

From a methodological point of view, this study demonstrates the effectiveness of models based on combinations of bands selected according to physical criteria, which facilitates their interpretation and extrapolation to other sensors with similar characteristics. Calibration and validation using in situ data reinforce the usefulness of this methodology as a complementary tool to traditional monitoring. Given that the selected water bodies have different trophic states and optical conditions, the spectral relationships obtained can be applied, with the necessary adaptations, to other lakes and reservoirs with similar characteristics, both in the Mediterranean basin and in regions with similar climates and trophic status.

The models developed provide a solid basis for remote monitoring of the carbon cycle in continental aquatic systems, a crucial aspect in the context of climate change and eutrophication.

5. Acknowledgments

The authors acknowledge the CIPROM/2021/49 project, entitled Remote Sensing Spectroscopy for wetlands BIOdiversity (RESSBIO), funded by the PROMETEU program of the Generalitat Valenciana.

6. References

Alvado, B., Sòria-Perpinyà. X., Caballero, G., Soria, J.M., Ruíz-Verdú, A., Delegido, J., Vicente, E., Rodrigo, M.A., Moreno, J. Comparación entre ACOLITE y productos L2 de los sensores PRISMA, DESIS y EnMAP en aguas interiores. In Proceeding of the XX Congreso de la Asociación Española de Teledetección, Cádiz, Spain, 5-7 June 2024.

Bonelli, A.G., Loisel, H., Jorge, D., Mangin, A., Fanton d'Andon, O., Vantrepotte, V. 2022: A new method to estimate the dissolved organic carbon concentration from remote sensing in the global open ocean. *Remote Sens. E.*, 281.

Cherukuru, N., Ford, P.W., Matear, R.J., Oubelkheir, K., Clementson, L.A., Suber, K., Steven, A.D.L. 2016: Estimating dissolved organic carbon concentrations in turbid coastal waters using optical remote sensing observations. *Int. J. Applied Earth Obs. Geoinfor.* 52, 149-154.

Hestir, E.L., Brando, V.E., Bresciani, M., Giardino, C., Matta, E., Villa, P., Dekker, A.G. 2015: Measuring freshwater aquatic ecosystems: the need for a hyperspectral global mapping satellite mission. *Remote Sens. Environ.*, 167, 181-185.

Hoge, F.E., Vodacek, A., Blough, N.V. 1993: Inherent optical properties of the ocean: retrieval of the absorption coefficient of chromophoric dissolved organic matter from fluorescence measurements. *Limn. and Oceanog.*, 38(7), 1349-1402.

Kaufmann, H., Sang, B., Storch, T., Segl, K., Foerster, S., Guanter, L., Erhard, M., Heider, B., Hofer, S., Honold, H., Penné, B., Bachmann, M., Habermeyer, M., Müller, A., Müller, R., Rast, M., Staenz, K., Straif, C., Chlebek, C. 2016: Environmental mapping and analysis program – A German hyperspectral mission, Book: Optical payloads for space mission, John Wiley & Sons, Ed., Chapter 7.

Krutz, D., Müller, R., Knodt, U., Günther, B., Walter, I., Sebastian, I., Säuberlich, T., Reulke, R., Carmona, E., Eckardt, A., Venus, H., Fischer, C., Zender, B., Arloth, S., Lieder, M., Neidhardt, M., Grote, U., Schrandt, F., Gelmi, S., Wotjkowiak, A. 2019: The instrument design of the DLR Earth Sensing Imaging Spectrometer (DESIS), *Sensors*, 19.
Kutser, T., Verpoorter, C., Paavel, B., Tranvik, L.J. 2015: Estimating Lake carbon fractions from remote sensing data. *Remote Sens. Eviron.*, 157, 138-146.

Mostafiz, C. 2017: Assessing interactions between estuary water quality and terrestrial land cover in hurricane events with multi-sensor remote sensing. *Electronic Theses and Dissertations*, 5688.

Odermatt, D., Gitelson, A., Brando, V.E., Schaepman, M. 2012: Review of constituent retrieval in optically deep and

complex waters from satellite imagery. *Remote Sens. Environ.* 118, 116-126.

Quevedo-Castro, A., Monjardín-Armenta, S.A., Plata-Rocha, W., Rangel-Peraza, J.G. 2024: Implementation of remote sensing algorithms to estimate TOC, Chl-a, and TDS in a tropical water body; Sanalona reservoir, Sinaloa, Mexico. *Environ. Monitoring and Assess.*, 196.

Schröder, T., Schmidt, S.I., Kutzer, R.D., Bernet, H., Stelzer, K. Friese, K., Rinke, K. 2024: Exploring spatial aggregations and temporal windows for water quality match-up analysis using Sentinel-2 MSI and Sentinel-3 OLCI data. *Remote Sens.*, 16(15).

Shao, T., Song, K., Du, J., Zhao, Y., Liu, Z. Zhang, B. 2016. Retrieval of CDOM and DOC using in situ hyperspectral data: A case study for potable waters in Northeast China. *J. Indian Soc. Remote Sens.*: 44(1), 77-89.

Spencer, R.G., Butler, K.D., Aiken, G.R. 2012: Dissolved organic carbon and chromophoric dissolved organic matter properties of rivers in the USA. *J. Geophys. Res.: Biogeosci.* 117.

Tehrani, N.C., D'Sa, E.J., Osburn, C.L., Bianchi, T.S., Schaeffer, B.A. 2013: Chromophoric dissolved organic matter and dissolved organic carbon from Sea-Viewing Wide Field-of-View sensor (SeaWiFS), Moderate Resolution Imaging Spectroradiometer (MODIS) and MERIS sensors: case study for the Northern Gulf of Mexico. *Remote Sens.*, 5, 1439-1464.

Toming, K., Kutser, T., Laos, A., Sepp, M., Paavel, B., Nöges, T. 2016: First experiences in mapping lake water quality parameters with Sentinel-2 MSI imagery. *Remote Sens.*: 8(8), 640.

Vanderklift M.A., Martinez, M., Butler, J.R., Coleman, M., Lawrence, A., Prislan, H. Thomas, S. 2019: Constraints and opportunities for market-based finance for the restoration and protection of blue carbon ecosystems. *Marine Policy*, 107: 103429.

Williamson, C., Dodds, W., Kratz, T., Palmer, M. 2008: Lakes and streams as sentinels of environmental change in terrestrial and atmospheric processes. *Front. Ecol. Environ.*, 6, 247-254.

Wong, J., Liew, S.C., Wong, E.W.S., Leong, S.C.Y. 2020: Estimation of colored dissolved organic matter using Sentinel-2 data in the coastal waters of Singapore. *J. Appl. Remote Sens.*, 14(3).

Zhang, Z., Zhu, W., Chen, J., Cheng, Q. 2021: Remotely observed variations of reservoir low concentration chromophoric dissolved organic matter and its response to upstream hydrological and meteorological conditions using Sentinel-2 imagery and Gradient Boosting Regression Tree. *Water Supp.* 21(2), 668-682.

Zhou, C., Zhou, M., Jia, R., Peng, Y., Zhao, F., Xu, R., Liang, S., Terada, A., Wang, G., Kinouchi, T., Xu, X. 2023: Particulate organic carbon potentially increases methane emissions from oxic water of eutrophic lakes. *Sci. Total Environ.*, 889.